Search Strategy for Rare Microstructure to Optimize Material Properties of Filled Rubber

Takashi Kojima (takashi.kojima02@y-yokohama.com)
Research and Advanced Development Division, The Yokohama Rubber Co., Ltd., 2-1 Oiwake, Hiratsuka Kanagawa 254-8601, Japan

Takashi Washio
Osaka University

Satoshi Hara
Osaka University

Masakata Koishi
Yokohama Rubber (Japan)

Research Article

Keywords: Markov chain Monte Carlo (MCMC), coarse-grained molecular dynamics (CGMD), high elastic modulus

Posted Date: January 21st, 2021

DOI: https://doi.org/10.21203/rs.3.rs-144773/v1

Search Strategy for Rare Microstructure to Optimize Material Properties of Filled Rubber

Takashi Kojima[1,2,*], Takashi Washio[2], Satoshi Hara[2], and Masataka Koishi[1]

[1] Research and Advanced Development Division, The Yokohama Rubber Co., Ltd., 2-1 Oiwake, Hiratsuka Kanagawa 254-8601, Japan

[2] Department of Reasoning for Intelligence, The Institute of Scientific and Industrial Research, Osaka University, 8-1, Mihogaoka, Ibarakishi, Osaka, 567-0047, Japan

*Corresponding author; email: takashi.kojima02@y-yokohama.com

Abstract

A shortcut to understand the microstructure-property relationship is sampling and analysis of microstructures that induce the desired material property. In the case of filled rubber, the simulation of complex filler morphology involves hundreds of filler particles. This requires a large amount of iterative sampling, because the number of parameters is $O(3n)$ when using coordinates of the n particles as the search objective. Furthermore, the morphology that induces the desired property, e.g. extremely high modulus, only occurs rarely. In this paper, we propose an effective three-step search method for the filler morphology. In the first step, the replica exchange Markov chain Monte Carlo (MCMC) was employed to discretely search among a wide range of morphologies. In this step, we reduced the filler morphology space in sampling by introducing distributed filler candidate points and spin function. In the second step, the gradient descent method was applied to search for the desired morphology locally in the high-dimensional space $O(3n)$, starting from the morphologies obtained by the replica exchange MCMC. Lastly, the coarse-grained molecular dynamics (CGMD) simulations were performed to validate the morphologies actually show the desired properties, because the surrogate model of CGMD was employed in the first 2 steps for the efficient search. Using the proposed method, we demonstrate the search for morphologies that induce high elastic modulus.

1. Introduction

Filled rubber is a composite material made of polymers and nanoscale fine filler particles, and their properties[1] are directly related to tire performance such as rolling resistance, abrasion resistance, and wet traction. To examine the strong dependencies between the mechanical properties and the filler morphologies, many researchers have applied X-ray scattering, electronic microscopy, and atomic force microscopy techniques [2,3,4,5,6,7,8,9]. However, the observations and experiments cannot clearly connect the structures with their effects. Computer simulations, on the other hand, can be used to visualize the inside of a tire and perform virtual experiments for tire design to improve the performance[10]. Coarse-grained molecular dynamics (CGMD) simulations of polymer materials have been performed to analyze the relationship between the nanometer-scale structures observed experimentally and the meter-scale mechanical properties[4,11,12,13,14,15,16]. However, several months of computation is often required to carry out a large-scale CGMD simulation that includes thousands of filler particles to analyze the nanometer-scale structures[17,18]. To the best of our knowledge, there have been no reports investigating the relationship based on many large-scale CGMD results.

The best way to study the relationship is sampling and analysis of filler morphologies to extract the common nanometer-scale structures or features that induce the desired material properties (e.g., high elastic moduli and low hysteresis). In this regard, we are unaware of any reported sampling technique of the filler morphology for large strain responses, whether based on CGMD or not. The two major barriers to filler morphology sampling are the huge computational cost and the lack of effective sampling techniques. To overcome the former, we have previously established a highly accurate surrogate model for the large-scale CGMD[19] of filled rubber. The details of the surrogate model will be explained here in a later section.

Sampling the filler morphology means creating new filler morphology candidates, measuring a material property, and selecting filler morphologies providing the desired property. Two types of methods have been suggested for generating possible filler morphologies: probabilistic methods such as generating filler positions based on the Poisson point process[20,21], and deterministic methods that directly determine each filler position. In the probabilistic methods, the stochastic parameters such as Poisson process intensity characterizing the filler morphology that induces the desired material properties are not easily searched, because material properties largely vary depending on the randomly sampled filler morphologies even under the same parameters. In the deterministic methods, the filler morphologies are fixed by the input parameters, which are the coordinates of each filler particle in a three-dimensional space. Nevertheless, the number of target parameters increases dramatically with the number of filler particles (n) as $O(3n)$, which prevents sufficient morphology sampling.

In this paper, we propose a novel morphology search method which is hybrid of the probabilistic

and deterministic methods. It is the combination of the surrogate model for the large-scale CGMD, a Markov chain Monte Carlo (MCMC) technique[22], a gradient descent method, and CGMD simulation. To the best of our knowledge, sampling techniques with MCMC have not been applied to the filler morphology search, although it was used for manufacturing[23]. When the filler morphology is sampled iteratively, it is desirable to use coordinates of filler particles as the search parameters instead of stochastic parameters, because the variations of stochastic trials are large when the stochastic parameters are used as described previously. However, parameter search that scales as $O(3n)$ is hardly feasible for large n due to the huge computational cost and the curse of dimensionality[24,25]. To overcome this problem, we specifically propose an efficient and effective technique to intensively sample filler morphology that induces desired material properties. This search is conducted by the replica exchange MCMC and the surrogate model-based simulation in a discrete representation space of the filler morphology. Once candidate filler morphologies predicted to provide good material properties are searched, they are updated by the gradient descent method using the surrogate model-based simulation in order to further find filler morphologies that is predicted to provide better desired properties. Finally, CGMD simulations are carried out to validate whether the searched filler morphologies actually provide the desired properties, because the properties evaluated during the search using the replica exchange MCMC and the gradient descent method are merely the predicted values by a convolutional neural network (CNN) based surrogate model for efficient search.

2. Problem setting

As a preliminary study, we investigated the relationship between filler morphology and stress at strain of 0.3 using a random sampling technique and CGMD simulation in order to obtain filler morphologies having high elastic modulus that improve tire abrasion resistance. The space size was 170[σ] × 170[σ] × 170[σ] (σ: unit length used in the CGMD), and radius of filler particles is 10[σ] in all morphologies. Stresses were calculated using the molecular dynamics simulation software LAMMPS[26]. Simulation conditions such as the elongation rate were described in our past paper[18]. The number of random samples were 5,000 where various filler morphologies were generated. Figure 1Figure 1 shows the result of this investigation. The increase of the elastic modulus along with the aggregation of more filler particles is observed which is consistent with our existing knowlegde[1,9]. The result included only one morphology exceeding stress 0.65. Even for the lower stress 0.6, only six morphologies exceeded this number. The filler morphologies having stress more than 0.65 are rarely found by the random sampling. However, this does not imply nonexistence of any filler morphologies having higher stress. There may be some other filler morphologies providing high stress.

Our sampling objective was to obtain filler morphologies that induce stress of 0.65 or higher. It is well known that the stress of filled rubber is roughly proportional to volume fraction of filler[27,28], and

filler particles percolate beyond approximately from 22 vol% to 25 vol%[29]. Moreover, mechanical properties change once filler particles percolate[30,31]. Based on these studies, the volume fraction of filler was restricted to 20 vol% represented by 250 filler particles during the search, in this study, in order to understand the mechanisms to generate the stress in a phase not having filler percolation as the first step of our project. The space size and the radius of filler particle were 170[σ] × 170[σ] × 170[σ] and 10[σ], respectively, same as the random sampling.

In a nutshell, the technical issues related to the sampling of filler morphologies are followings:

1. Iterative CGMD simulations were owing to huge amount of computation resource.
2. There was no an efficient and effective sampling technique in the high-dimensional space $O(3n)$.

We have developed a highly accurate surrogate model of CGMD simulation of filled rubber based on our past study[19] to alleviate the former problem, and its details are explained in the next section. In this study, we propose the novel hybrid sampling approach to overcome the latter problem.

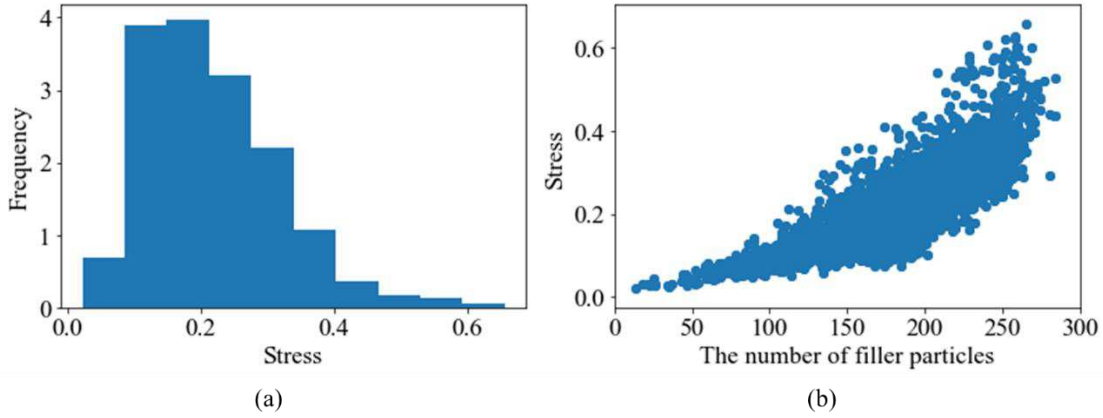

Figure 1. Result of the random sampling: (a) is the distribution of stress at strain of 0.3, and (b) is a plot of the number of filler particles and stress.

3. Our previous work

Our proposed method for sampling filler morphology is based on MCMC, which is an effective and sequential sampling technique for high-dimensional probability distributions. To search a high-dimensional space densely, at least tens of thousands of samples and their evaluations are required. However, CGMD simulations cannot afford sampling all these filler morphologies, because it requires huge amount of computation resource. In our previous work, we have developed a surrogate model for CGMD simulation of filled rubber, which used a CNN to replace the CGMD simulation in highly

accurate approximation[19]. We were able to drastically reduce the computation cost from one month to one minute to derive the material properties. In the present paper, this surrogate model was used for high-speed simulation of the material property during the sampling.

3.1 Training data

Forty-five large-scale CGMD simulations of the filled rubber were performed to generate the training data set. The filler configurations were determined stochastically using multi-step Poisson point processes, in order to achieve effective distribution of the aggregated structures[20]. First, both the aggregate regions (where filler particles could be placed) and exclusion polymers (where the filler particles were not placed) were designated based on the aggregate radius, the volume fraction of the exclusion polymer, and the stochastic input parameters of Poisson point process intensity for the both the aggregate and the exclusion polymer. The Poisson point process intensity were used to derive the number of the aggregate and the exclusion polymer. Second, a thousand filler particles were placed in the aggregate region based on two input parameters: the volume fraction and particle radii of filler particle. We selected parameters that likely produce high elasticity based on our prior knowledge, because we aimed to sample the high-elasticity morphologies. Specifically, many papers have reported that the elastic modulus increases when the filler particles are aggregated[1,9,17,18,32,33]. Hence, small values were used for the aggregate radius and the Poisson point process intensity for the aggregate. Meanwhile, a large volume fraction and small Poisson point process intensity were applied for the exclusion polymer, because the fraction of the aggregate region is small in the aggregated structure of the filler particles. Figure 2 represents the 4 input parameter distributions of the filler configurations. CGMD input files representing the filler morphologies derived by this process were created, and deformation simulations up to a strain of 0.3 were carried out using the molecular dynamics simulation software LAMMPS[26]. Figure 3 shows a visualized filler morphology among 45 filler morphologies.

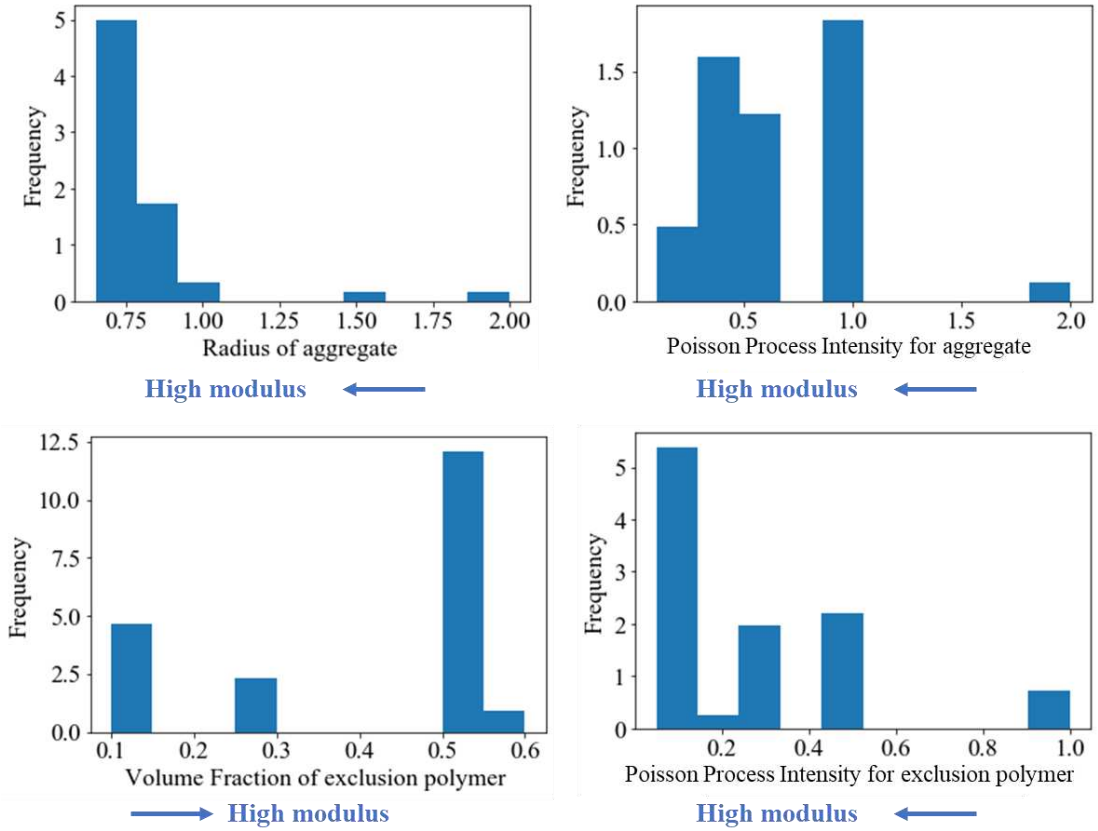

Figure 2. Distributions of four input parameters for filler morphology to generate the training data for the CNN-based surrogate model.

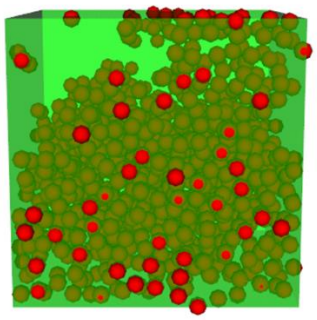

Figure 3. Example of visualized filler configuration. The green box is the entire region of the large-scale CGMD simulation. The red particles are the filler particles.

The training data which composed of filler morphology image at strain of 0.0 and stress at strain of 0.3 were generated from these CGMD results for the CNN-based surrogate model. The information in the local region, not the entire CGMD region, were converted to the training data, with the aim of data augmentation. A total of 92,000 training data instances were generated through the selection of the

local regions and the adoption of their mirror images. The local region had 1/2 length of x, y, and z dimensions of the entire CGMD region, respectively. Thus, the volume of the local region was 1/8 of the entire CGMD region. Some reports have shown that the filler morphology in filled rubber has a hierarchal structure ranging from nanometer- to micrometer-scale[2,4,7,34] and the filler-filler interaction is partially responsible for the stress[1,18,35,36]. Therefore, the stress arises from not only the filler particles inside the considered region but also nearby filler particles outside the region. To establish a surrogate model that considers particles both inside and outside the given region, we generated training data consisting of the filler morphology in a given local region and its surrounding region by extracting them from large-scale CGMD results. Figure 4 presents a schematic drawing of the training data instance. Hence, the trained CNN-based surrogate model outputs the estimated stress in the local region at strain of 0.3 from the input filler morphology image at strain of 0.0.

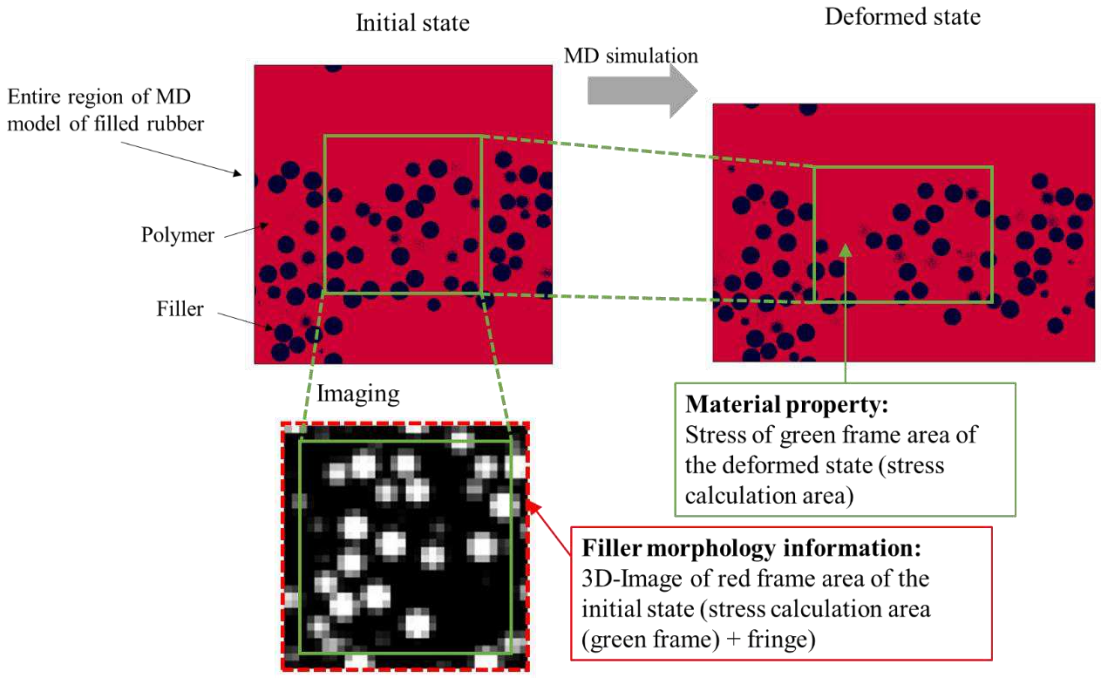

Figure 4. Schematic for training data instance which composed of the imaged filler morphology information and the material property. The material property results from the large-scale CGMD simulation.

3.2 Training of the CNN-based surrogate model

The surrogate model was constructed by 3D-CNN using PyTorch with two convolutional layers and one fully connected layer, and trained by minimizing a mean squared error between the value resulted by the CGMD simulation and the value estimated by the model. The number of features in both convolutional layers was 50. The kernel of size 4×4×4 moved with a stride of 1 in both convolutional layers. The pooling size of the first convolutional layer was 2, and the global average pooling[37] was

used to connect the second convolutional layer to the fully connected layer. A leaky rectified linear unit (leaky ReLU[38]) was used as the activation function to avoid zeroing signals during training. Detailed conditions such as the learning rate were described in our previous study[19]. Figure 5 represents the prediction performance of the CNN-based model. It shows that the prediction accuracy up to the stress 0.6 was sufficiently high. By assuming good extrapolation accuracy of this model toward the stress equal to and slightly more than 0.65, this model was used as the function that calculates the stress from filler morphology in the present study.

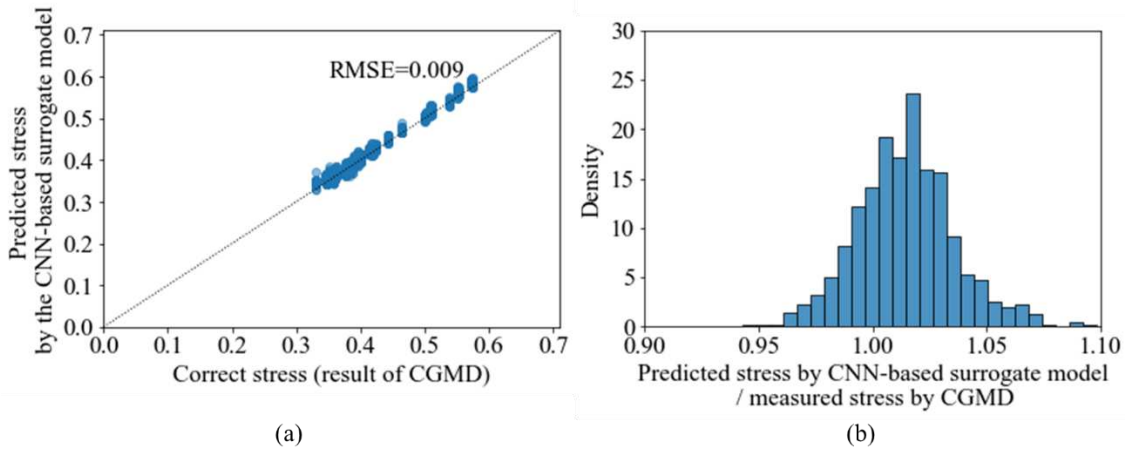

Figure 5. Predictive performance of the CNN-based surrogate model for 250 filler particles: (a) presents the comparison between the correct stress and the predicted stress, and (b) is the histogram of the prediction accuracy of the stress.

4. Proposed method

The multicanonical MCMC[39] and the replica exchange MCMC[40] are sampling techniques for rare events. The multicanonical MCMC uses a single MCMC technique that sequentially draws samples from an implicitly given probability distribution in a possibly high-dimensional space. Weights for the samples are iteratively updated to ensure their uniform distribution with respect to the feature of interest. Accordingly, it could efficiently produce samples meeting specific conditions including rare target conditions, with their weights precisely preserving their probabilities. The replica exchange MCMC employs layered MCMCs in parallel. The MCMC sequence in the top layer follows the probability distribution of interest by maintaining its detailed balance of the sequence. The deeper layers follow more flattened distributions in the same manner, respectively. Samples in the pairwise

layers are exchanged under a detailed balance in order to widely search for rare events. In this study, the replica exchange MCMC capable of simultaneous parallel searches was employed for sampling filler morphology, because our purpose was to obtain as many morphologies as possible.

4.1 Replica exchange MCMC for filler morphology search

The replica exchange MCMC draws samples from T probability distributions in parallel, where each distribution has parameter θ_t ($t = 1, \cdots, T$) and T is total number of temperatures. The search area of each MCMC sequence in the sample spaces depend on the inverse temperature θ_t when the probability distribution follows the Boltzmann distribution. A low temperature is used in the top layer to locally search for rare conditions of interest, while the deeper layers with higher temperatures search wider areas in the sample space because their distribution is wider than the top layer. Occasional exchange of the samples enables to search for local solutions in the wide sample space. In this study, the probability distribution $P(S^t)$ of the filler morphology S at temperature t is designed using the Boltzmann distribution as follows:

$$\mathrm{E}(S^t) = \frac{1}{\lambda f(S^t)}, \tag{1}$$

$$P(S^t) = exp\left(-\frac{E(S^t)}{\alpha_t}\right). \tag{2}$$

where, $f(\cdot)$ is the function that calculates the stress from filler morphology S^t. The surrogate model for the CGMD of filled rubber based on our previous study was used to calculate $f(S^t)$. The energy $E(S^t)$, which is inversely proportional to the stress, is designed to have higher probability of generating morphologies that provide greater stresses. Each MCMC sequence searches the filler morphology space iteratively, following the different probability distributions that depend on the temperature via the coefficient α_t. λ is a hyper parameter to tune the dependency of the probability distributions on the stresses. In the high-temperature sequence, filler morphologies are iteratively searched according to a flattened state distribution, so that a wide filler morphology space is searched without being trapped in local solutions. In contrast, the low-temperature sequence focuses on the local search for rare filler morphologies by following the probability distribution near the target stress f_{th}. That is, it iteratively searches for rare filler morphology without significantly changing the filler morphology characteristics. In addition, the change in filler morphology at high temperatures is reflected in the sequence at low temperature via the exchange between their sequences. Thus, the replica exchange MCMC can be used to obtain many local solutions, including rare filler morphologies that provide high stresses, from the wide filler morphology space. This suggests that we efficiently obtain the local solutions searched in all temperature sequences by analyzing the sequence history of the low temperature $t = 1$. In this study, the filler morphologies providing the maximum stress in the continuous MCMC sequence steps at $t = 1$ were extracted as the candidate initial filler morphologies

in the subsequent gradient decent search. The detail will be described later in the subsection 4.2.

Each MCMC sequence of the replica exchange MCMC tracks the transition of filler morphology S_n^t following the target distribution $P(S_n^t)$ where S_n^t is filler morphology at step n. Let $\mathrm{Q}(\mathrm{S}^t|S_n^t)$ and $\mathrm{Q}(S_n^t|\mathrm{S}^t)$ be the transition probabilities from the filler morphology S_n^t to S^t and from S^t to S_n. S^t is a candidate filler morphology of step $n+1$ at temperature t. The acceptance of S^t is determined as follows:

$$S_{n+1}^t = \begin{cases} \mathrm{S}^t & if \ \dfrac{\mathrm{P}(\mathrm{S}^t)\mathrm{Q}(S_n^t|\mathrm{S}^t)}{\mathrm{P}(S_n^t)\mathrm{Q}(\mathrm{S}^t|S_n^t)} > r, \\ S_n^t & otherwise \end{cases} \tag{3}$$

where $\mathrm{r}\sim P_U([0,1])$ is sampled from a uniform distribution.

The exchange of S_n^t and S_n^{t+1}, that is, the exchange of filler morphologies between the adjacent temperatures t and $t+1$ sequences, was attempted at every m steps of n, i.e., $\{n|n \ mod \ m = 0 \ for \ all \ n \in N\}$, under the detailed balance, where m is sufficiently larger than the relaxation periods of the sequences. Here, *N* represents the number of total sequence steps.

$$\text{randomly choose } t \in T-1, \tag{4}$$

$$Swap(S_n^t, S_n^{t+1}) \ \ if \ \frac{P(S_n^{t+1}|t)P(S_n^t|t+1)}{P(S_n^t|t)P(S_n^{t+1}|t+1)} > r, \tag{5}$$

where $P\left(S_n^t\middle|t'\right)$ is the probability of the filler morphology S_n^t at temperature t'.

As mentioned above, our purpose is to sample the filler morphology represented by the coordinates of the filler particle centers. Thus, the sampled parameter space for 250 particles has 250×3 = 750 dimensions (the x, y, and z coordinates of 250 particles). The search of 750 dimension is hardly performed, because of so called the curse of dimensionality. To overcome this issue, we reduce the search space by introducing a spin function that indicates the filler morphology, and then searched for filler morphology in the reduced search space. Specifically, filler candidate points were distributed in the space, and the state of each point was controlled by the spin function. Given $\mathrm{X} \subset R^3$ be the set of filler candidate positions, the state of each filler candidate point $x \in \mathrm{X}$: $\mathrm{s}(x)$ is defined as follows:

$$\mathrm{s}(x) = \begin{cases} 1 & if \ x \ is \ filler, \\ -1 & otherwise. \end{cases} \tag{6}$$

The filler morphology S_n^t is represented by $S_n^t = \{s(x)|x \in X\} \in \{1,-1\}^{|X|}$ s.t. $|\{x \in X|s(x)=1\}| = N_{filler}$, where N_{filler} is the number of filler particles. The candidate point x representing filler is in $\{x \in X|s(x)=1, s(x) \in S_n^t\}$. The filler morphology is updated during the search following the procedure described below. First, randomly selected point with $s(x)=1$ changes into the polymer state $s(x)=-1$. Then, a randomly selected point *y* in the polymer state, $s(y)=-1$, is changed into the filler $s(y)=1$ if its distance from point x is d or

less so that point y is described as follows:

$$y \in X_n^-(x|S_n^t) = \{y \in X | \|y - x\| < d, s(y) = -1, s(y) \in S_n^t\}. \quad (7)$$

The transition probability $\mathrm{Q}(\mathrm{S}^t|S_n^t)$ from the current filler configuration S_n^t to the new configuration $\mathrm{S}^t = \{s(x) = -1,\ s(y) = 1,\ s(z) \in S_n^t$ is unchaged for all $z \neq x, y\}$ is as follows:

$$\mathrm{Q}(\mathrm{S}^t|S_n^t) = \frac{1}{|X_n^-(x|S_n^t)|}. \quad (8)$$

4.2 Filler morphology search using the gradient descent method

The second step employs the gradient descent method to search for the desired filler morphologies, starting from an initial filler morphology S. Every S is the candidate initial morphology providing the maximum stress in its interval of the MCMC sequence at $t = 1$. The interval is the period between the successive replica exchanges of the MCMC sequences at $t = 1$ and $t = 2$. The details are shown in Figure 6.

Given a parameter vector $X(S)$ which is the concatenations of 3-dimensional continuous position vectors x_i of all filler particles $i = 1, \ldots, N_{filler}$ in a filler morphology S, $X(S)$ is iteratively updated during the gradient descent search. This search enables us to sample the filler morphologies with more desired property than the candidates resulted by the replica exchange MCMC. The mini-batch gradient descent method[41,42] is employed to update $X(S)$ of every candidate filler morphology S:

$$X(S) \leftarrow X(S) - \eta \mathrm{g}, \quad (9)$$

$$\mathrm{g} = \frac{1}{|B|} \sum_{i \in B} \frac{\partial f(S)}{\partial x_i}, \quad (10)$$

where $\mathrm{B}, \eta,$ and g are the mini-batches of fillers, the learning rate, and the gradient, respectively. Note that the gradient $\partial f(S)/\partial x_i$ of the filler particle x_i is measured as follows:

$$\frac{\partial f(S)}{\partial x_i} = \frac{f\big(x_i + \delta|X(S)\big) - f\big(x_i - \delta|X(S)\big)}{2\delta}, \quad (11)$$

where δ is the virtual displacement of the filler particle and $f\big(x_i + \delta|X(S)\big)$ is f where all $x \in X(S)$ except x_i is fixed. The update of the filler position is repeated until $f\big(X(S)\big)$ exceeded the threshold, $f_{th} < f\big(X(S)\big)$ or fall into the local solution, that is, $f\big(X(S)\big)$ converges.

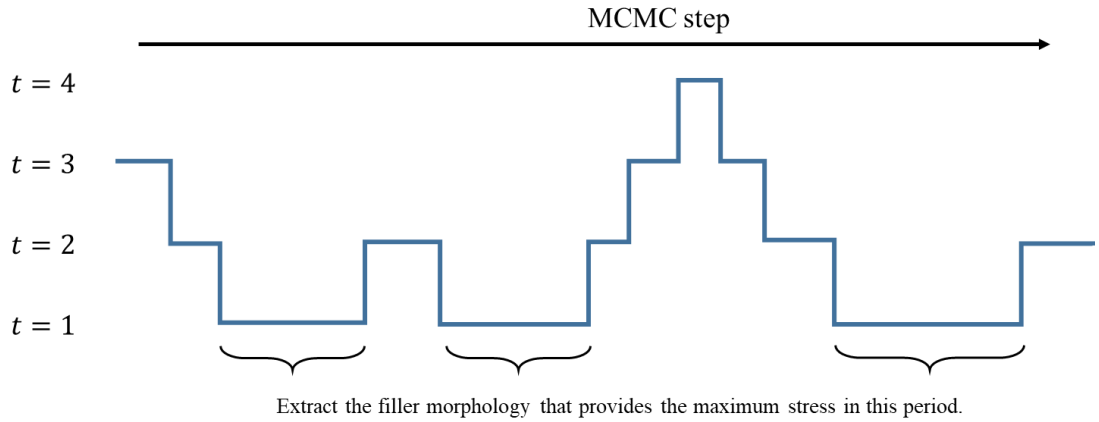

Figure 6. Schematic for extracting filler morphologies used as an initial state in the gradient descent method from a history of replica exchange MCMC. Three morphologies were extracted in this example history.

Figure 7 is a schematic drawing of the proposed method that combines the replica exchange MCMC and the gradient descent method for the filler morphology search.

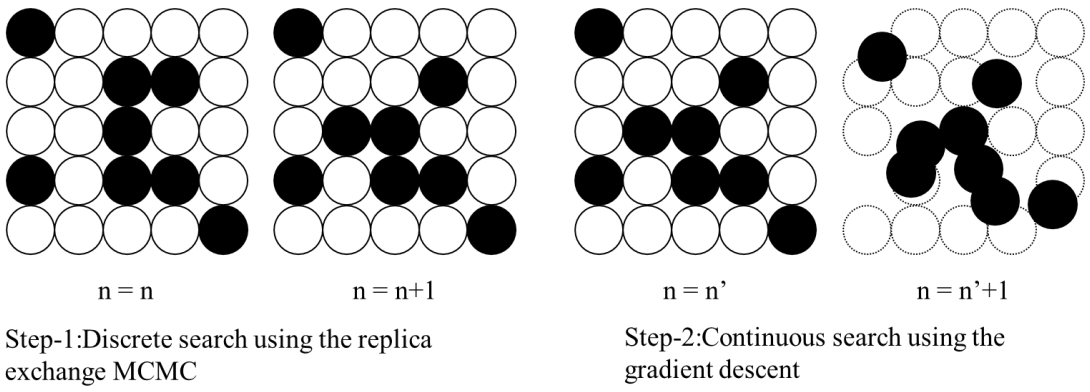

Figure 7. Schematic drawing of the proposed method. Circles in the step-1 represent the filler candidate positions. Open circles and filled circles are polymer and filler, respectively. The left figure in the step-2 is the initial state of this step. The right figure shows an updated filler configuration.

4.3 Validation simulation of the mechanical property using CGMD

Stresses evaluated during the search using the replica exchange MCMC and the gradient descent method are values predicted by the CNN-based surrogate model for the effective search. Accordingly, the high stresses of the filler morphologies provided by the search is not ensured, and thus the validation of the high stress values of these filler morphologies is performed by using CGMD in the last step.

5. Result and discussion

5.1 Sampling performance

Sampling performance of the proposed method was compared with those of random sampling method, combined method of random sampling and gradient descent, and method using replica exchange MCMC only. The random sampling provides the baseline performance. The combined method of random sampling and gradient descent shows the effect of the gradient descent, and the last method shows the effect of the replica exchange MCMC. Every sampling method was applied using the computation resource of 10,000[node×hour]. As described in the previous section, every search trial employed 250 filler particles, and the goal was to find the filler morphologies providing the stress over 0.65 in terms of CGMD result. A total of 12×12×12=1,728 filler candidate points were set in a grid manner, that is, 12 points were set in each of x, y, and z directions at equal intervals, to define a filler morphology in every trial. The radius of the filler was 10[σ], same as in the previous study[19]. In the random sampling, 250 of the 1,728 candidate filler points were randomly selected as fillers. In the combined method of the random sampling and the gradient descent, the randomly selected filler coordinates were improved by the gradient descent until the stress converged as described in the subsection 4.2. In the method using the replica exchange MCMC, 4 parallel MCMC sequences were employed. Figure 8 presents the target distributions $P(S^t)$ defined in Equation (2). The parameter α_t in Equation (2) reflecting the temperature t to the distribution was set to $(\alpha_1, \alpha_2, \alpha_3, \alpha_4) = (0.5, 2.5, 10, 70)$. The hyper parameter λ in Equation (1) was set to $1/8$. $P(S^{t_1})$ was designed to search the filler morphologies having higher stress, whereas $P(S^{t_4})$ was designed to search the wider filler morphology space. $P(S^{t_2})$ and $P(S^{t_3})$ were set to largely overlap with the distributions of the other layers to introduce the frequent replica exchanges between these layers which enhance search efficiency. Parameter d in Equation (7), which was the threshold of the neighbor filler candidate points, was 30[σ]. First 5,000 steps of the MCMC sequence were abandoned for burn-in, and the exchanges of filler morphologies between the adjacent temperature sequences were attempted every 3,000 MCMC steps. The learning rate η in Equation (9), mini-batch size B in Equation (10), and virtual displacement δ in Equation (11) for measuring the gradient in the gradient descent were 5, 1.0, and 0.1[σ] (1/100 of the filler radius), respectively. CGMD simulations were performed with 1020 cpus using a HPCI system.

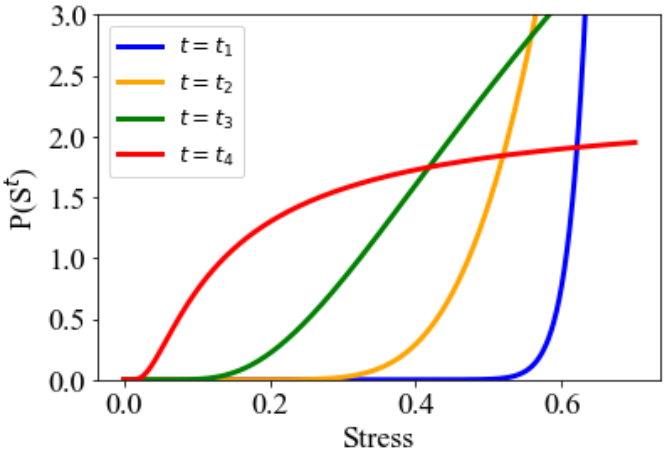

Figure 8. Target distributions of each temperature.

Table 1 and Figure 9 present the comparison of the sampling performances. Table 1 shows the number of the sampled filler morphologies providing the CGMD measured stress equal to or larger than 0.65, and the averages of the CGMD measured stresses over all sampled filler morphologies. Figure 9 shows distributions of the CGMD measured stresses. The histogram of each method was drawn by the CGMD measured stresses of twenty morphologies randomly sampled from the morphologies resulted by the method. The random sampling, which provides the baseline performance, did not find filler morphologies providing the stress over 0.65, and the average stress of sampled morphologies was the smallest. Both the gradient descent method and the replica exchange MCMC method could find the morphologies providing larger stress than the random sampling, but only one morphology having the stress over 0.65 was obtained by the replica exchange MCMC. Whereas, the proposed method combining the replica exchange MCMC and the gradient descent found eleven morphologies over 0.65. This result demonstrates the high sampling efficiency of the proposed method. In the proposed method, 20 morphologies were presumed to provide large stress over 0.65 by the CNN-based surrogate model, and 11 morphologies among the twenty provided CGMD measured stress over 0.65. This result indicated the extrapolation predictability of the CNN-based surrogate model, while the CNN was the interpolation model of the training instances providing the stresses up to 0.6 as described in the section 3.

Table 1. Performance comparison of the random sampling method, the combined method of the random sampling and the gradient descent, the method using the replica exchange

MCMC only, and the proposed method.

Sampling technique	The number of the sampled filler morphologies providing CGMD measured stress of 0.65 or larger.	Average of CGMD measured stresses.
Random sampling method	0	0.33
Combined method of random sampling and gradient decent	0	0.46
Replica Exchange MCMC	1	0.52
Proposed method (replica exchange MCMC and gradient decent)	11	0.66

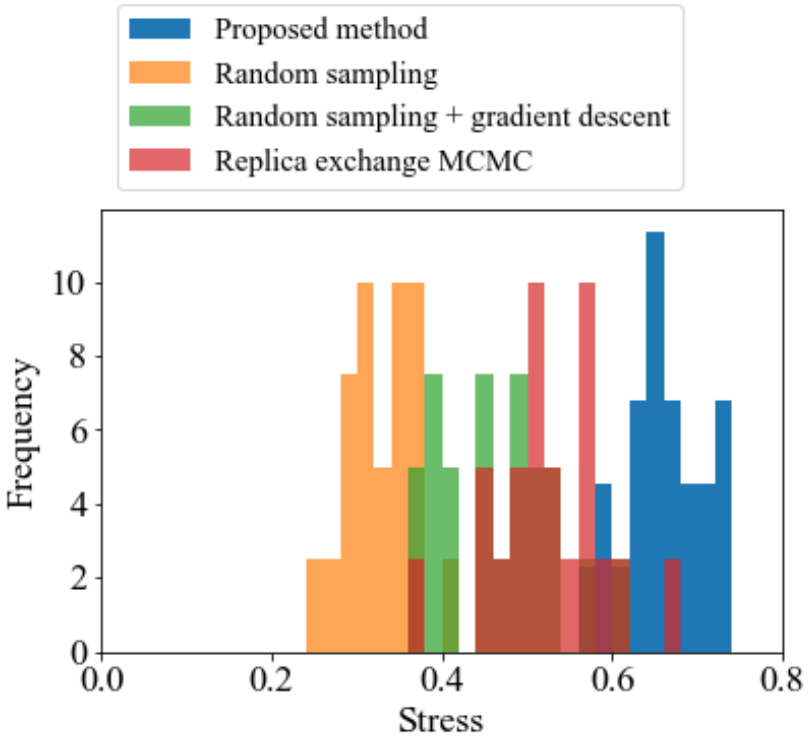

Figure 9. Distribution of the CGMD measured stress of the morphologies obtained by each method.

5.2 Comparison of the filler morphology

The filler morphologies providing the GCMD measured stress over 0.65 sampled by the proposed method were compared with the morphologies providing the stress over 0.6 sampled by the random sampling in the section 2. Filler morphologies were quantified by persistent homology (PH) and visualized using persistent diagram (PD)[43,44,45,46,47]. Persistent homology is a mathematical method for investigating the hidden structure from complex data, and has been applied to analyze polymerized material[45]. Suppose that there are k balls at $z_1, z_2, \cdots, z_k$ as shown in Figure 10 (a). In this study, we present each filler by a ball with a radius r. $k = 250$ represents the number of fillers, and z_i represents a coordinate of the center of i-th filler particle. All balls are disconnected, as shown in Figure 10 (a), when r is small. As r increase to r_1, the balls coalesce to "birth" a loop, as shown in Figure 10 (b). Furthermore, the empty space surrounded by the loop is completely covered by the balls, if $r = r_2$ where the balls meet at the "death" position denoted by the cross mark in Figure 10 (c), and the loop disappears. This example shows that a loop has a "birth" length, $b = r_1^2$, and "death" length, $d = r_2^2$, and the loop exists only when $b < r^2 < d$. PH is the map from $\{z_1, z_2, \cdots, z_k\}$ to $\{(b_1, d_1), (b_2, d_2), \cdots, (b_l, d_l)\}$, where l is the number of the loops formed by the k fillers in a space. The result of PH analysis is visualized in a scatter plot of (b_i, d_i) as shown in Figure 10 (d), and this plot is the PD. Figure 11 (a) displays the PDs of six morphologies providing the stress over 0.6, which were obtained by the random sampling in the section 2, and Figure 11 (b) displays the PDs of three morphologies providing the stress over 0.65, which were obtained by the proposed method. Comparing the PDs depicted that the proposed method could sample filler morphologies not obtained by the random sampling. The morphologies obtained by the proposed method obviously show longer life time (difference between death length and birth length) in the PDs. This is resulted by the significant difference of the death length distributions between the proposed method and the random sampling method rather than their difference of the birth length distributions. This fact implies that the morphologies obtained by the proposed method comprise of larger aggregates of filler particles than the morphologies obtained by the random sampling. In addition, some morphologies obtained by the proposed method have greater aggregates whose birth lengths and death lengths are beyond 0.5 and 0.7, respectively. This variety of aggregate sizes suggests that hierarchical aggregate structure is a key to induce the larger stress of filled rubber. Such complex structures were hardly found by the random

sampling.

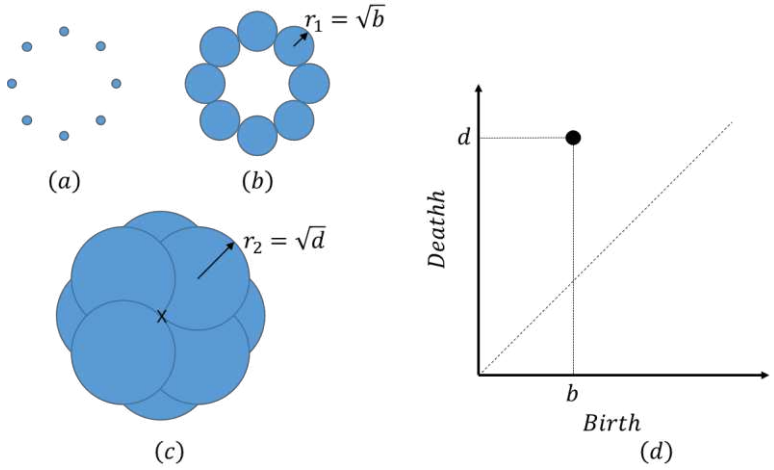

Figure 10. Schematic drawing of persistent homology. (a) Balls are disconnected when radius of ball r is smaller than r_1. (b) A loop emerges at $r = r_1 = \sqrt{b}$. (c) The loop disappears at $r = r_2 = \sqrt{d}$. (d) Persistent diagram representing the result of persistent homology analysis.

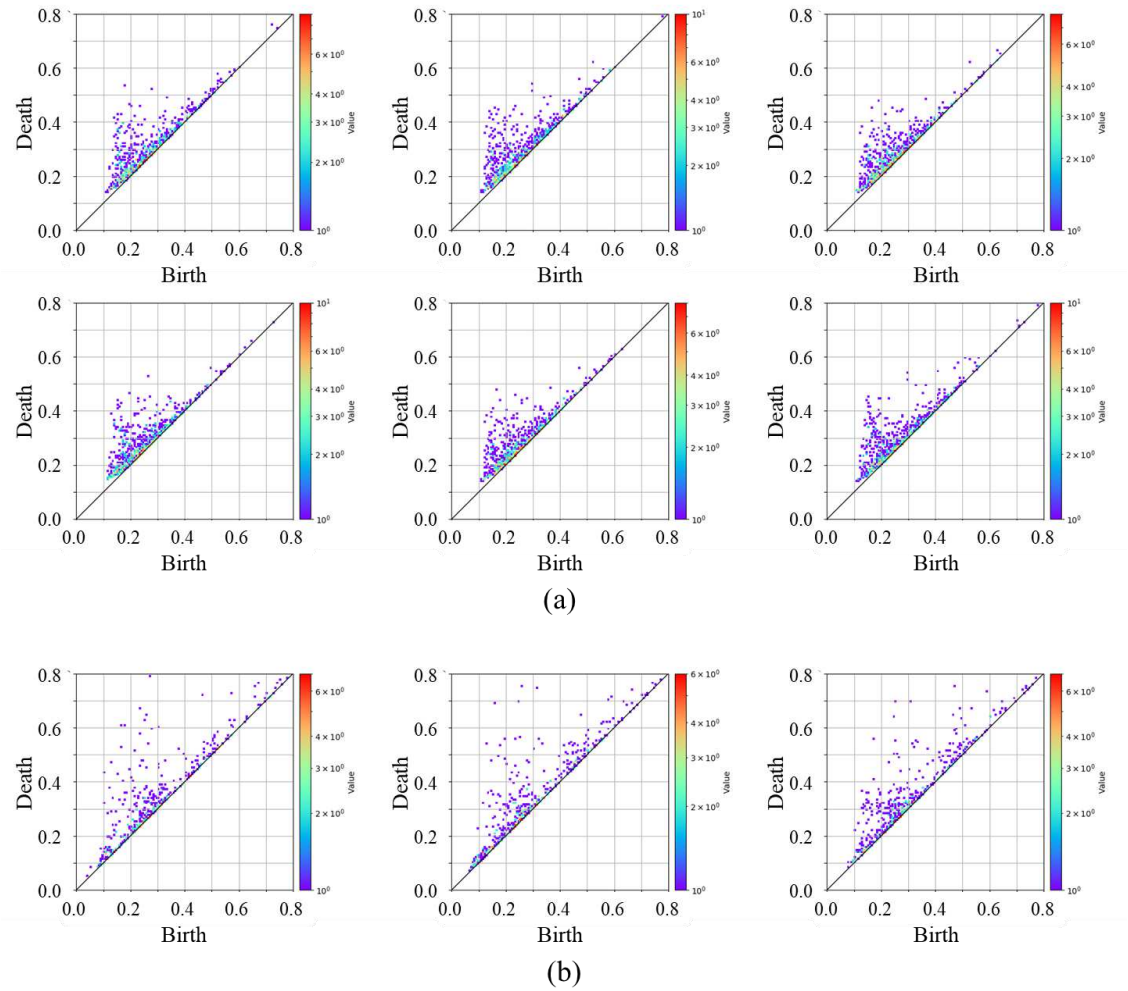

Figure 11. Persistent diagrams: (a) filler morphologies obtained by the random sampling, the morphology on the upper left provided the stress over 0.65, while the other morphologies provided the stress from 0.6 to 0.65, and (b) filler morphologies, which provided the stress over 0.65, sampled by the proposed method.

6 Conclusion

We proposed a novel approach searching for high-stress filler morphologies. It is a hybrid of the probabilistic and deterministic search methods. The approach is the combination of the surrogate model deriving the stress, the replica exchange MCMC, the gradient descent, and the CGMD

simulation. In the search using the replica exchange MCMC, we reduced the search space dramatically by introducing discrete filler candidate positions and the spin state at the candidate points. The filler morphologies are searched by the replica exchange MCMC with the surrogate model and updated by the surrogate model based gradient descent in order to further find filler morphologies that provide better property. The CGMD simulations were lastly performed to validate whether the sampled morphologies actually show the desired property.

We demonstrated the higher sampling efficiency of the proposed method than these of the random sampling method, the combined method of random sampling and gradient descent, and the method using replica exchange MCMC only. Through the comparisons of the filler morphologies obtained by the proposed method and the random sampling method, we demonstrated the possibility that the filler morphologies having the hierarchical aggregate structures of the fillers have high stress.

In future wok, we will acquire many morphologies using the proposed method, analyze the common structures or features among the high-stress morphologies, and reveal keys for controlling the elastic modulus. A search under a larger filler volume fraction than 20vol% where filler particles percolate is also a subject of our future work. Moreover, a study on the morphology composed of multiple filler types is another subject of our future work, while we focused on the filler morphology composed of a unique filler type in this study. In addition, the enhancement of the extrapolation predictability of the CNN-based surrogate model should be attempted in future work. The proposed method can be widely applied to many microstructured materials, and will contribute to the advancement of materials science in many areas.

References

1. T.A.Vilgis, G.Heinrich, M. K. *REINFORCEMENT OF Polymer Nano-Composites -Theory, Experiments and Applications-*. (Cambridge University Press, 2009).
2. Hashimoto, T., Amino, N., Nishitsuji, S. & Takenaka, M. Hierarchically self-organized filler particles in polymers: cascade evolution of dissipative structures to ordered structures. *Polym. J.* **51**, 109–130 (2019).
3. Nakajima, K., Ito, M., Nguyen, H. K. & Liang, X. Nanomechanics of the rubber-filler interface. *Rubber Chem. Technol.* **90**, 272–284 (2017).
4. Smith, J. S., Bedrov, D. & Smith, G. D. A molecular dynamics simulation study of nanoparticle interactions in a model polymer-nanoparticle composite. *Compos. Sci. Technol.* **63**, 1599–1605 (2003).
5. Klüppel, M. The role of polymer confinement between filler particles in rubber reinforcement. **110**, 41801 (2013).
6. Starr, F. W., Douglas, J. F. & Glotzer, S. C. Origin of particle clustering in a simulated polymer nanocomposite and its impact on rheology. *J. Chem. Phys.* **119**, 1777–1788 (2003).

7. Dannenberg, E. M. Effects of Surface Chemical Interactions on the Properties of Filler-Reinforced Rubbers. *Rubber Chemistry and Technology* vol. 48 410–444 (1975).
8. Lorenz, H. & Klüppel, M. Microstructure-based modelling of arbitrary deformation histories of filler-reinforced elastomers. *J. Mech. Phys. Solids* **60**, 1842–1861 (2012).
9. Klüppel, M. The Role of Disorder in Filler Reinforcement of Elastomers on Various Length Scales. *Adv. Polym. Sci.* **164**, 1–86 (2003).
10. Koishi, M., Miyajima, H. & Kowatari, N. Conceptual design of tires using multi-objective design exploration. *11th World Congr. Comput. Mech. WCCM 2014, 5th Eur. Conf. Comput. Mech. ECCM 2014 6th Eur. Conf. Comput. Fluid Dyn. ECFD 2014* 3180–3189 (2014).
11. Silva Bellucci, F. *et al.* Morphological characterization by SEM, TEM and AFM of nanoparticles and functional nanocomposites based on natural rubber filled with oxide nanopowders. *Mater. Sci. Forum* **798–799**, 426–431 (2014).
12. Raos, G. & Casalegno, M. Nonequilibrium simulations of filled polymer networks: Searching for the origins of reinforcement and nonlinearity. *J. Chem. Phys.* **134**, 1–14 (2011).
13. Hagita, K., Morita, H. & Takano, H. Molecular dynamics simulation study of a fracture of filler-filled polymer nanocomposites. *Polymer (Guildf).* **99**, 368–375 (2016).
14. Patil, S. P., Rege, A., Sagardas, Itskov, M. & Markert, B. Mechanics of Nanostructured Porous Silica Aerogel Resulting from Molecular Dynamics Simulations. *J. Phys. Chem. B* **121**, 5660–5668 (2017).
15. Smith, S. M. & Simmons, D. S. Horizons for design of filled rubber informed by molecular dynamics simulation. *Rubber Chem. Technol.* **90**, 238–263 (2017).
16. Raos, G., Moreno, M. & Elli, S. Computational experiments on filled rubber viscoelasticity: What is the role of particle - Particle interactions? *Macromolecules* **39**, 6744–6751 (2006).
17. Hagita, K., Morita, H., Doi, M. & Takano, H. Coarse-Grained Molecular Dynamics Simulation of Filled Polymer Nanocomposites under Uniaxial Elongation. *Macromolecules* **49**, 1972–1983 (2016).
18. Kojima, T. & Koishi, M. Influence of filler dispersion on mechanical behavior with large-scale coarse-grained molecular dynamics simulation. *Tech. Mech.* **38**, 41–54 (2018).
19. Kojima, T., Washio, T., Hara, S. & Koishi, M. Synthesis of computer simulation and machine learning for achieving the best material properties of filled rubber. *Sci. Rep.* **10**, (2020).
20. Figliuzzi, B. *et al.* Modelling the microstructure and the viscoelastic behaviour of carbon black filled rubber materials from 3D simulations. *Tech. Mech.* **36**, 32–56 (2016).
21. Omeiza, D., Speakman, S., Cintas, C. & Weldermariam, K. Smooth Grad-CAM++: An Enhanced Inference Level Visualization Technique for Deep Convolutional Neural Network Models. 1–10 (2019).
22. Hastings, W. K. Monte carlo sampling methods using Markov chains and their applications.

Biometrika **57**, 97–109 (1970).

23. Kisamori, K., Washio, T., Kameda, Y. & Fujimaki, R. A rare and critical condition search technique and its application to telescope stray light analysis. *SIAM Int. Conf. Data Mining, SDM 2018* 567–575 (2018) doi:10.1137/1.9781611975321.64.
24. LeCun, Y., Bottou, L., Bengio, Y. & Haffner, P. Gradient-based learning applied to document recognition. *Proc. IEEE* **86**, 2278–2323 (1998).
25. Kasim, M. F. *et al.* Up to two billion times acceleration of scientific simulations with deep neural architecture search. 1–10 (2020).
26. Plimpton, S. Short-Range Molecular Dynamics. *J. Comput. Phys.* **117**, 1–42 (1997).
27. E. Guth. Theory of Filler Reinforcement. *Rubber Chem. Technol.* **18**, 596–604. (1945).
28. D., I., Lee. The Viscosity of Concentrated Suspensions. *Transactions of the Society of Rheology **13**,* 273 (1969)
29. Jiwen, L., Benxin, L., Yehua J., Xiaojuan Z., Guangshui Y., Chong S, & Shugao Z. Investigation of filler network percolation in carbon black (CB) filled hydrogenated butadiene-acrylonitrile rubber (HNBR), *Polymer Bulletin* (2020).
30. CHONG, S., ZHANG, P., WRANA, C., SCHUSTER, R. & ZHAO, S. COMBINED DIELECTRIC AND MECHANICAL INVESTIGATION OF FILLER NETWORK PERCOLATION BEHAVIOR , FILLER – FILLER CONTACT , AND FILLER – POLYMER INTERACTION ON CARBON BLACK – FILLED HYDROGENATED ACRYLONITRILE – BUTADIENE RUBBER. *RUBBER Chem. Technol.* **87**, 647–663 (2014).
31. Karasek, L., Meissner, B., Asai, S. & Sumita, M. Percolation Concept : Polymer-Filler Gel Formation , Electrical Conductivity and Dynamic Electrical Properties of Carbon-Black-Filled Rubbers. **28**, 121–126 (1996).
32. Oda, H., Kiyohara, S., Tsuda, K. & Mizoguchi, T. Transfer learning to accelerate interface structure searches. *J. Phys. Soc. Japan* **86**, 210–213 (2017).
33. Kopal, I., Labaj, I., Harničárová, M., Valíček, J. & Hrubý, D. Prediction of the tensile response of carbon black filled rubber blends by artificial neural network. *Polymers (Basel).* **10**, (2018).
34. MIHARA, S. Insight into Chemical Reaction and Reinforcement Mechanism of Silica Filled Rubber During Processing. *Nippon Gomu Kyokaishi* **88**, 425–430 (2015).
35. Kojima, T. & Koishi, M. Mechanisms of Mechanical Behavior of Filled Rubber by Coarse-Grained Molecular Dynamics Simulations. *Tire Sci. Technol.* 1–30 (2020) doi:10.2346/tire.20.160117.
36. Ismail, H. & Ahmad, Z. Effect of a multifunctional additive on curing characteristics and mechanical properties of carbon blacks filled natural rubber compounds. *Iran. Polym. J. (English Ed.* **5**, 207–212 (1996).
37. Lin, M., Chen, Q. & Yan, S. Network in network. *2nd Int. Conf. Learn. Represent. ICLR 2014 -*

Conf. Track Proc. 1–10 (2014).

38. Maas, A. L., Hannun, A. Y. & Ng, A. Y. Rectifier nonlinearities improve neural network acoustic models. *ICML Work. Deep Learn. Audio, Speech Lang. Process.* **28**, (2013).
39. Iba, Y., Saito, N. & Kitajima, A. Multicanonical MCMC for Sampling Rare Events. 1–10 (2013) doi:10.1007/s10463-014-0460-2.
40. Earl, D. J. & Deem, M. W. Parallel tempering: Theory, applications, and new perspectives. *Phys. Chem. Chem. Phys.* **7**, 3910–3916 (2005).
41. Peng, X., Li, L. & Wang, F.-Y. Accelerating Minibatch Stochastic Gradient Descent Using Typicality Sampling. *IEEE Trans. Neural Networks Learn. Syst.* 1–11 (2019) doi:10.1109/tnnls.2019.2957003.
42. Robbins, H. & Monro, S. A Stochastic Approximation Method. *Ann. Math. Stat.* **22**, 400–407 (1951).
43. Herbert, E., David, L. & Afra, Z. Topological Persistence and Simplification. *Discret. Comput Geom* **533**, 511–533 (2002).
44. Zomorodian, A. Computing Persistent Homology. (2013) doi:10.1007/s00454-004-1146-y.
45. Obayashi, I. & Hiraoka, Y. Persistence Diagrams with Linear Machine Learning Models.
46. Hiraoka, Y., Nakamura, T., Hirata, A., Escolar, E. G. & Matsue, K. Hierarchical structures of amorphous solids characterized by persistent homology. **113**, 7035–7040 (2016).
47. Ichinomiya, T., Obayashi, I. & Hiraoka, Y. Persistent homology analysis of craze formation. **012504**, 1–6 (2017).

Acknowledgements

This research used computational resources of the HPCI system provided by Nagoya Univ. and by Kyoto Univ. through the HPCI System Research Projects (Project ID: hp190034 and hp200056).

Author Contributions

T.K. conceived this work and performed all simulations and analyses. All authors discussed the obtained results. T.K. wrote the first version of the manuscript. All authors have given approval to the final version of the manuscript.

Competing interests

The authors declare no competing interests.

Figure Legends

Figure 1. Result of the random sampling: (a) is the distribution of stress at strain of 0.3, and (b) is a plot of the number of filler particles and stress.**Error! Reference source not found.**

Figure 2. Distributions of four input parameters for filler morphology to generate the training data for the CNN-based surrogate model.

Figure 3. Example of visualized filler configuration. The green box is the entire region of the large-scale CGMD simulation. The red particles are the filler particles.

Figure 12. Schematic for training data instance which composed of the imaged filler morphology information and the material property. The material property results from the large-scale CGMD simulation.

Figure 13. Predictive performance of the CNN-based surrogate model for 250 filler particles: (a) presents the comparison between the correct stress and the predicted stress, and (b) is the histogram of the prediction accuracy of the stress.

Figure 14. Schematic for extracting filler morphologies used as an initial state in the gradient descent method from a history of replica exchange MCMC. Three morphologies were extracted in this example history.

Figure 15. Schematic drawing of the proposed method. Circles in the step-1 represent the filler candidate positions. Open circles and filled circles are polymer and filler, respectively. The left figure in the step-2 is the initial state of this step. The right figure shows an updated filler configuration.

Figure 16. Target distributions of each temperature.

Figure 17. Distribution of the CGMD measured stress of the morphologies obtained by each method.

Figure 18. Schematic drawing of persistent homology. (a) Balls are disconnected when radius of ball r is smaller than r_1. (b) A loop emerges at $r = r_1 = \sqrt{b}$. (c) The loop disappears at $r = r_2 = \sqrt{d}$. (d) Persistent diagram representing the result of persistent homology analysis.

Figure 19. Persistent diagrams: (a) filler morphologies obtained by the random sampling, the morphology on the upper left provided the stress over 0.65, while the other morphologies provided the stress from 0.6 to 0.65, and (b) filler morphologies, which provided the stress over 0.65, sampled by the proposed method.

Tables

Table 2. Performance comparison of the random sampling method, the combined method of the random sampling and the gradient descent, the method using the replica exchange MCMC only, and the proposed method.

Sampling technique	The number of the sampled filler morphologies providing CGMD measured stress of 0.65 or larger.	Average of CGMD measured stresses.
Random sampling method	0	0.33

Combined method of random sampling and gradient decent	0	0.46
Replica Exchange MCMC	1	0.52
Proposed method (replica exchange MCMC and gradient decent)	11	0.66

Figures

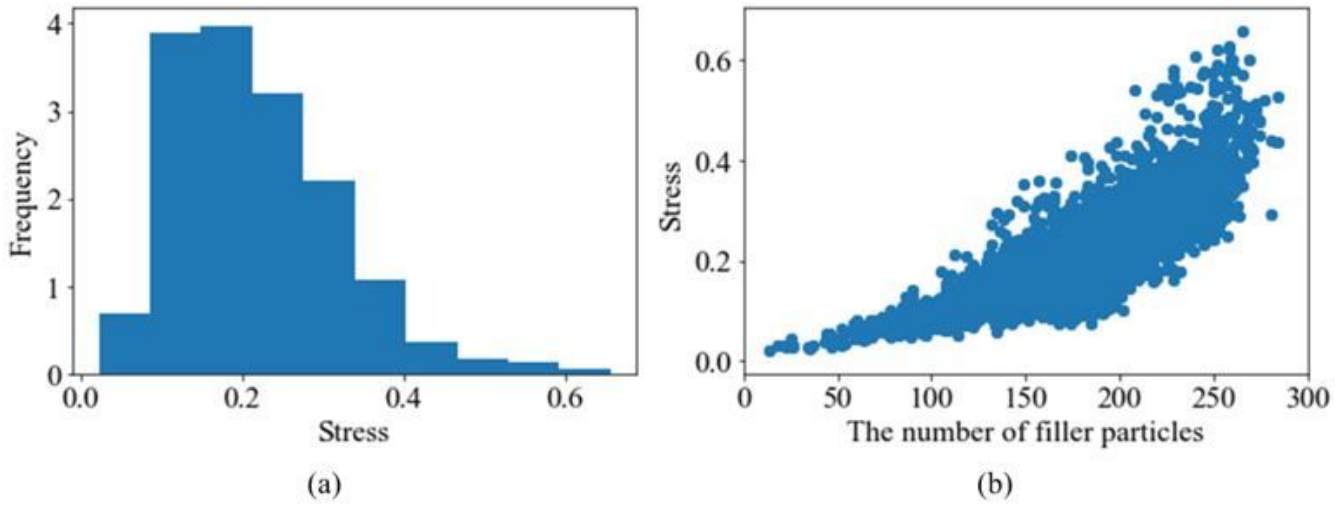

Figure 1

Result of the random sampling: (a) is the distribution of stress at strain of 0.3, and (b) is a plot of the number of filler particles and stress.

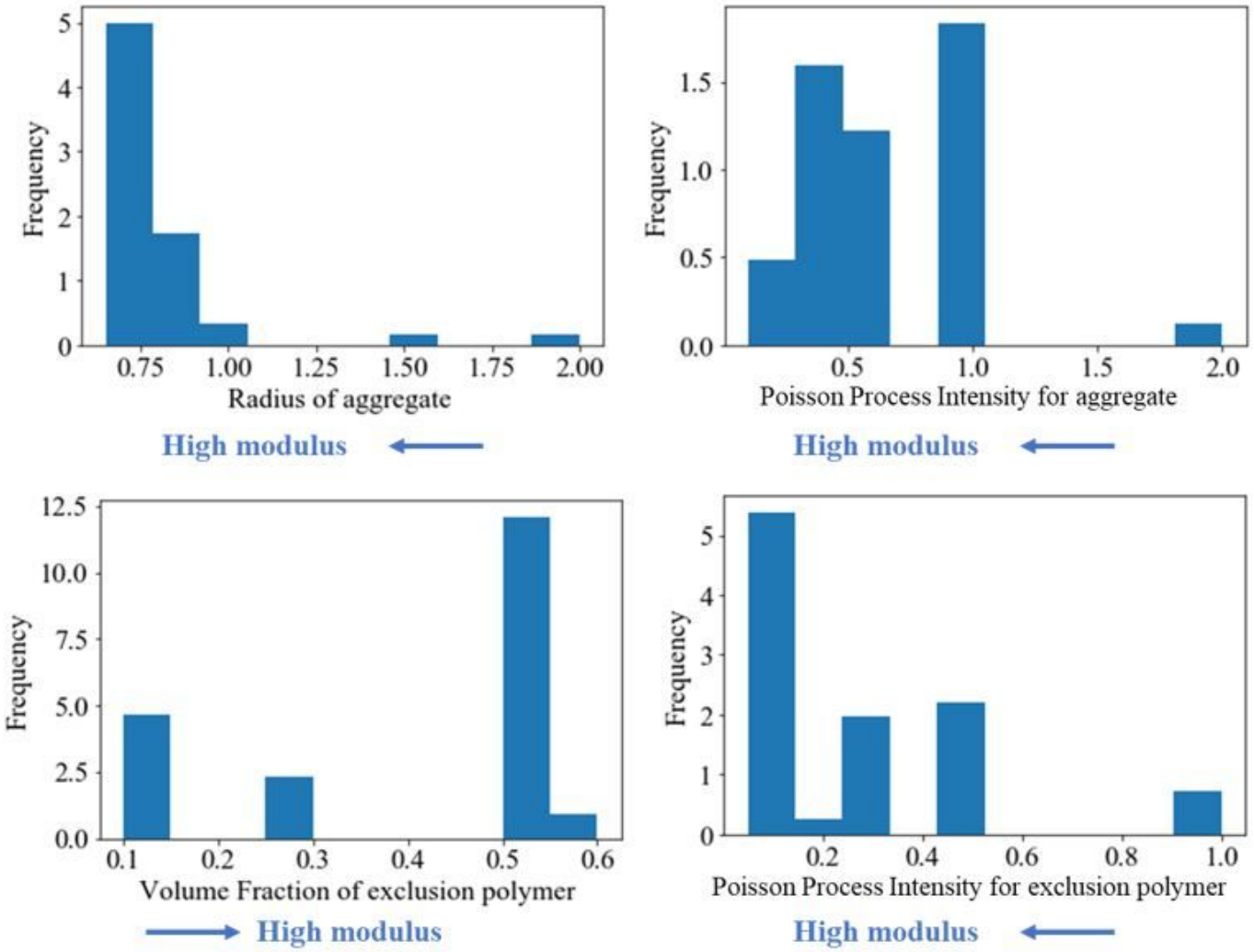

Figure 2

Distributions of four input parameters for filler morphology to generate the training data for the CNN-based surrogate model.

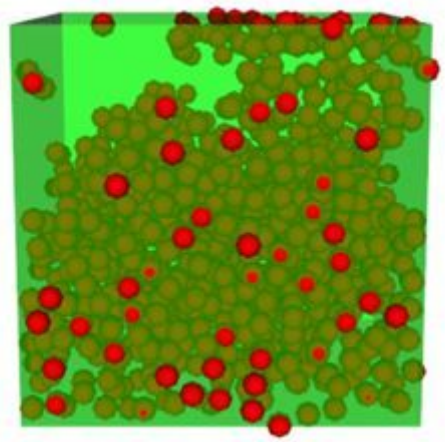

Figure 3

Example of visualized filler configuration. The green box is the entire region of the large-scale CGMD simulation. The red particles are the filler particles.

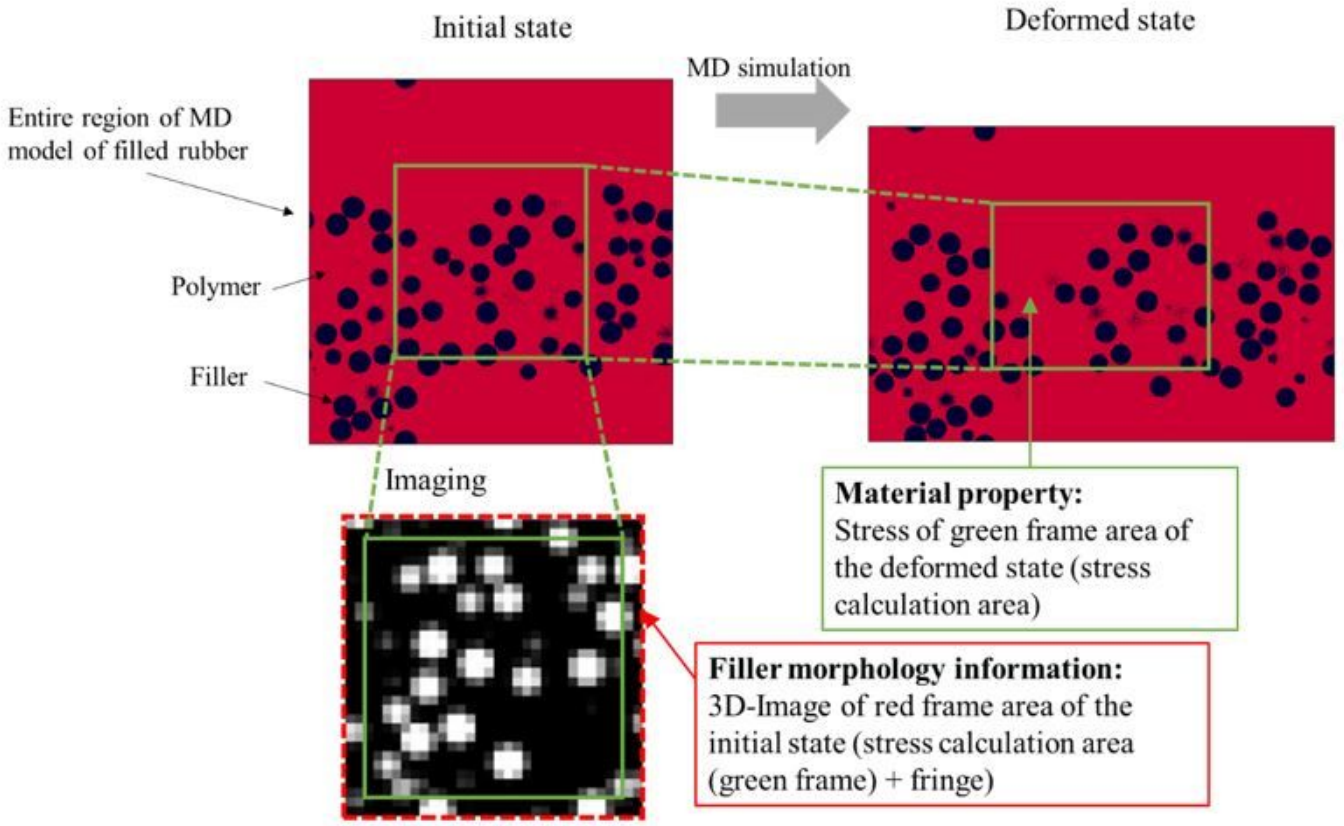

Figure 4

Schematic for training data instance which composed of the imaged filler morphology information and the material property. The material property results from the large-scale CGMD simulation.

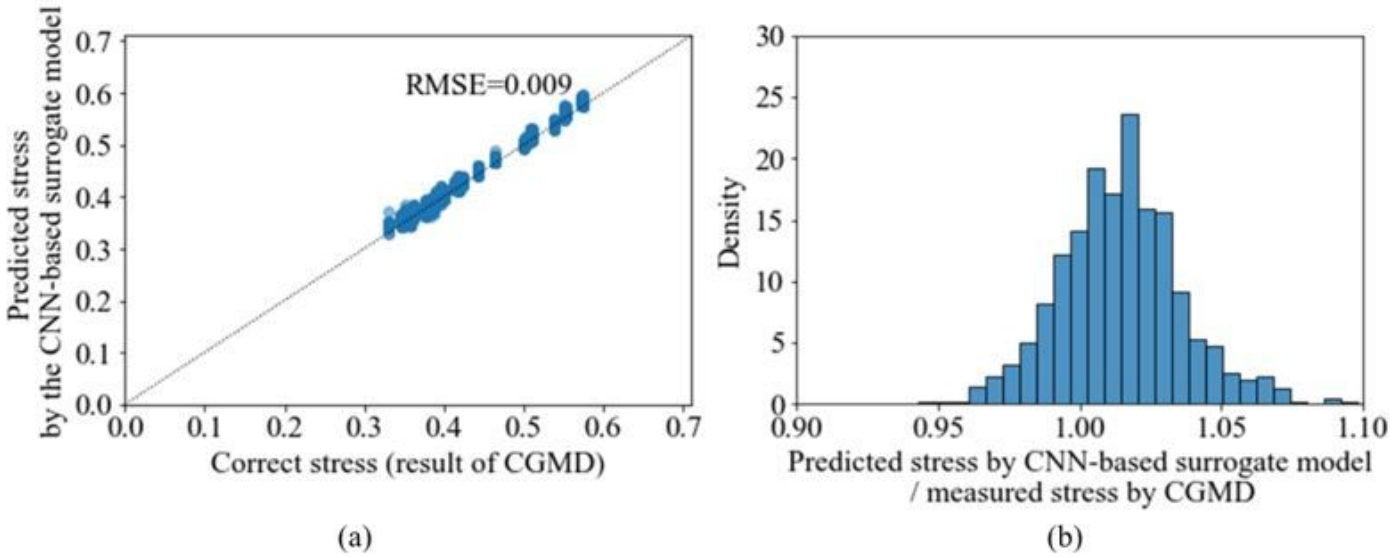

Figure 5

Predictive performance of the CNN-based surrogate model for 250 filler particles: (a) presents the comparison between the correct stress and the predicted stress, and (b) is the histogram of the prediction accuracy of the stress.

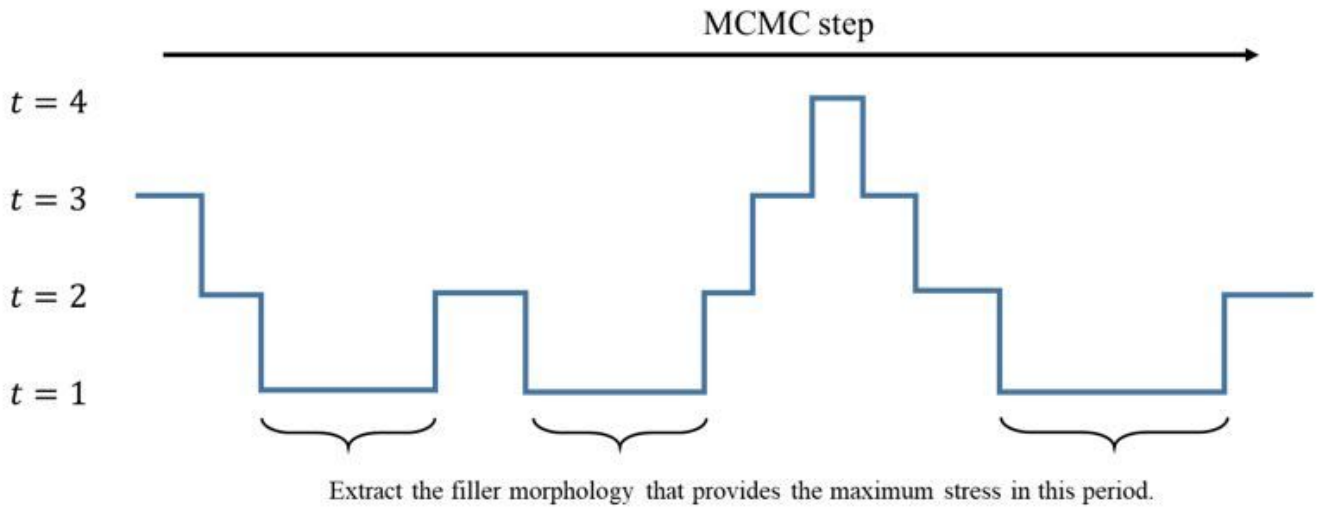

Figure 6

Schematic for extracting filler morphologies used as an initial state in the gradient descent method from a history of replica exchange MCMC. Three morphologies were extracted in this example history.

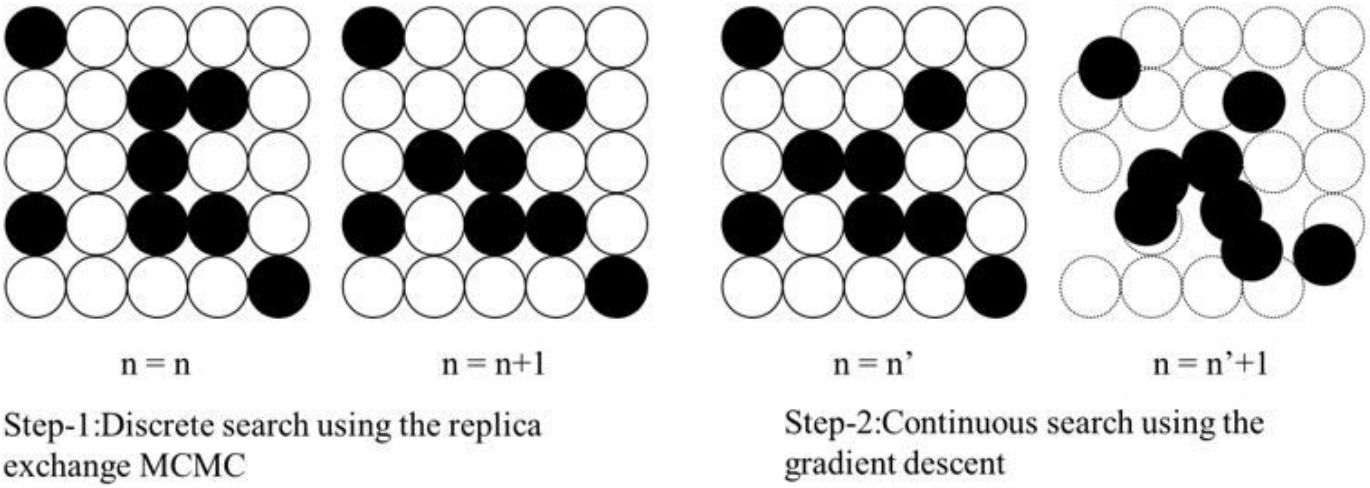

Figure 7

Schematic drawing of the proposed method. Circles in the step-1 represent the filler candidate positions. Open circles and filled circles are polymer and filler, respectively. The left figure in the step-2 is the initial state of this step. The right figure shows an updated filler configuration.

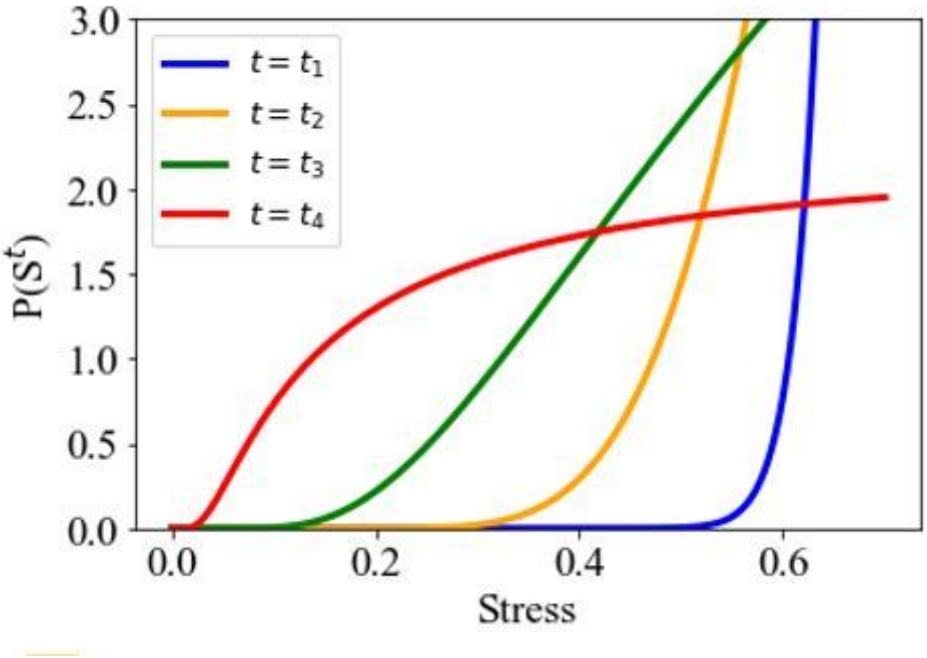

Figure 8

Target distributions of each temperature.

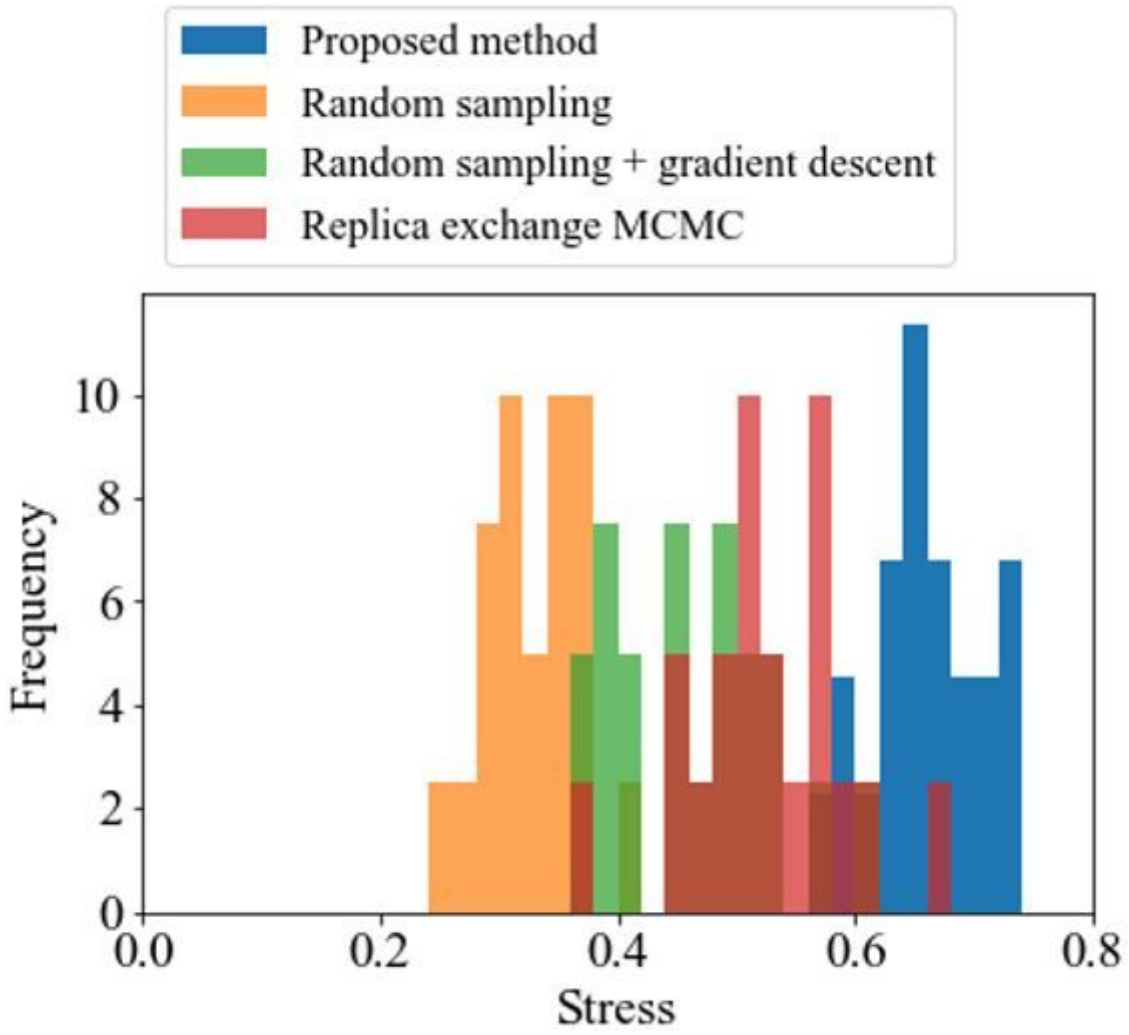

Figure 9

Distribution of the CGMD measured stress of the morphologies obtained by each method.

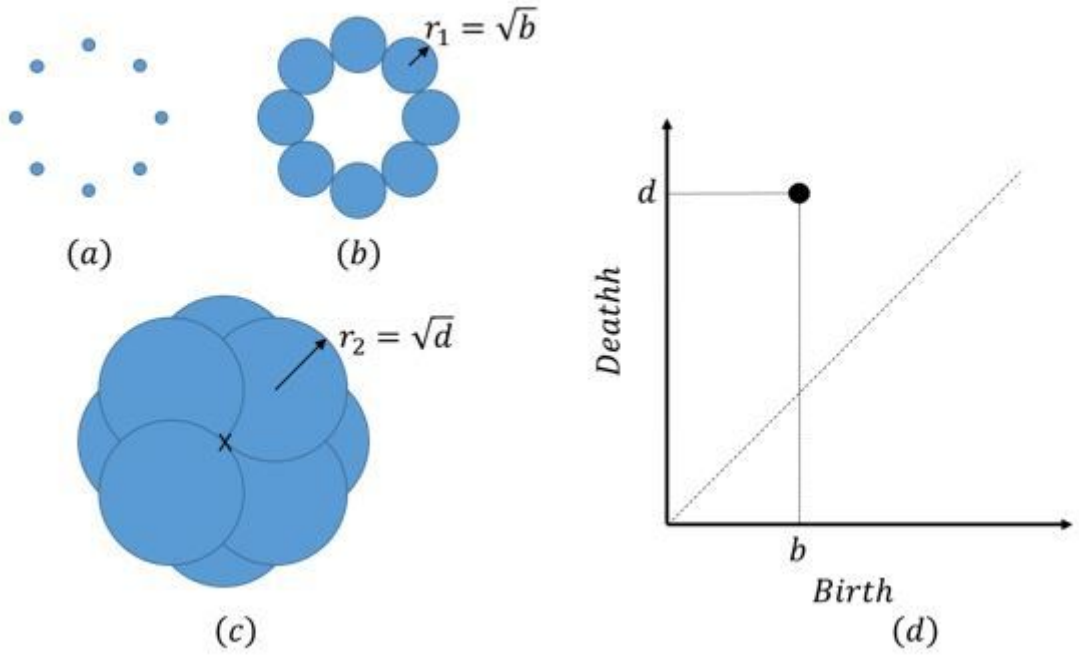

Figure 10

Schematic drawing of persistent homology. (a) Balls are disconnected when radius of ball r is smaller than r1. (b) A loop emerges at r = r1 = √b. (c) The loop disappears at r = r2 = √d. (d) Persistent diagram representing the result of persistent homology analysis.

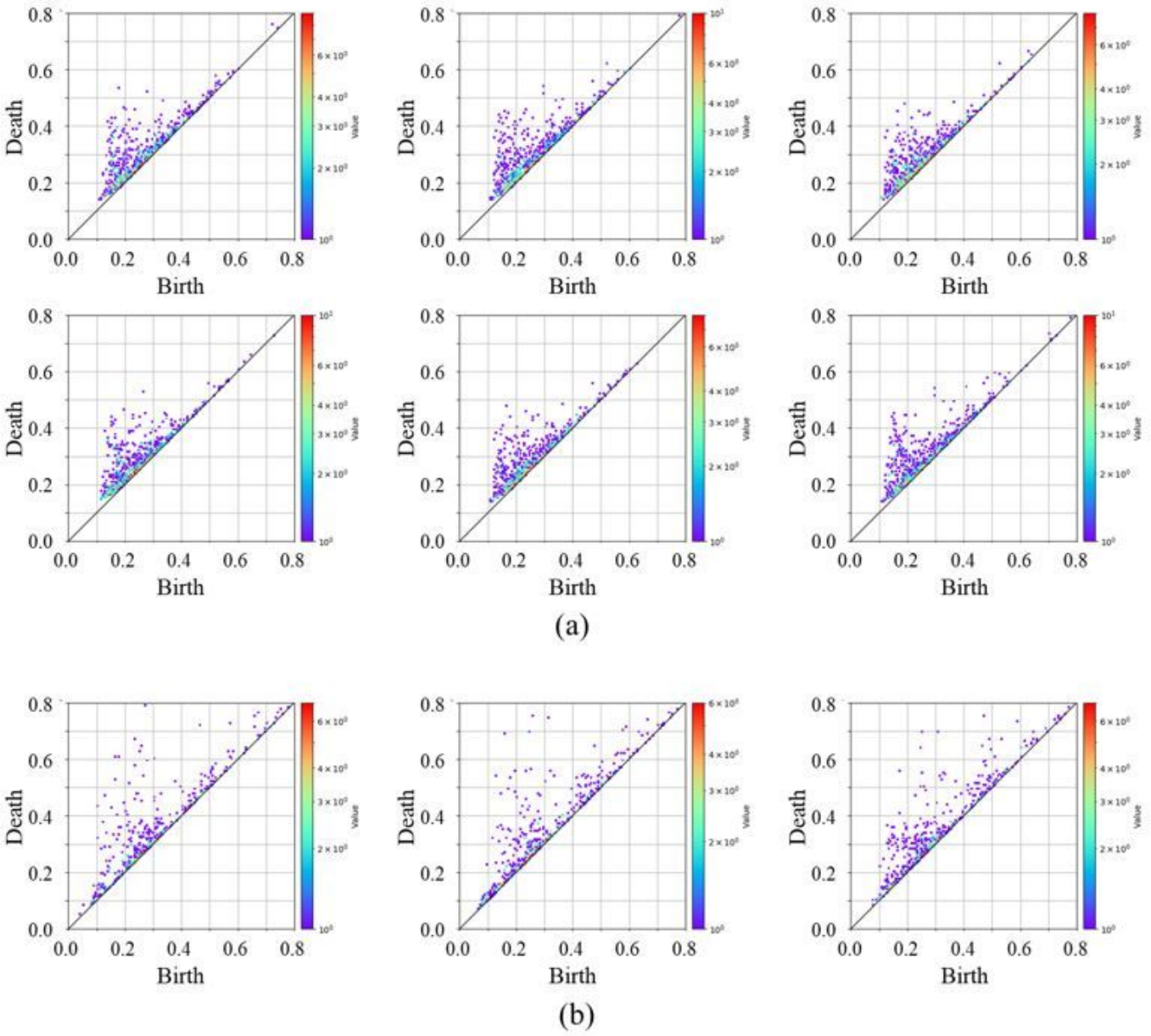

Figure 11

Persistent diagrams: (a) filler morphologies obtained by the random sampling, the morphology on the upper left provided the stress over 0.65, while the other morphologies provided the stress from 0.6 to 0.65, and (b) filler morphologies, which provided the stress over 0.65, sampled by the proposed method.